JOTCS A
Journal of the Turkish Chemical Society
Section: A
Chemistry

TURKISH CHEMICAL SOCIETY

# Determination of Gluconate Binding Properties on Magnetite Surface and Investigation of Carboxymethylation and Hydrazination Mechanisms of the Gluconated Magnetite Surface: A Computational Study

**Işılay ÖZTÜRK[a]*, Şenay ŞANLIER[b], Armağan KINAL[a]**

aEge University, Faculty of Science, Department of Chemistry 35100 Bornova IZMIR, TURKEY

bEge University, Faculty of Science, Department of Biochemistry 35100 Bornova IZMIR, TURKEY

**Abstract:** In the present study, the probable binding structure of a gluconate molecule with magnetite, ($Fe_3O_4$) nanoparticles, as well as, carboxymethylation and hydrazination mechanisms of the gluconate bound to the iron oxide surface have been computationally investigated by the DFT-B3LYP method. The B3LYP/LanL2DZ calculations together with experimental IR data available revealed that the probable binding structure of gluconate is bidentate bridged binding to the magnetite surface. The carboxymethylation and hydrazination mechanisms of gluconate were calculated at B3LYP/6-31+G(d,p) level of theory. The results indicate that the reaction between gluconate and chloroacetate in aqueous medium has one step mechanism passing through a low activation barrier (12.3 kcal/mol) with a reaction enthalpy of −42.8 kcal/mol. In addition, hydrazone bond formation reaction of the gluconate bound to the iron oxide surface has a highly-exothermic two-step-mechanism with barriers of 7.1 and 2.4 kcal/mol, respectively, in water. The activation barrier of the overall reaction is accepted as the barrier of the first step since the barrier of this step is greater than that of the second one. Consequently, it can be predicted that both carboxymethylation and hydrazination reactions should be spontaneous under moderate conditions.

**Keywords:** Magnetite nanoparticles, Gluconate, Binding properties, Carboxymethylation, Hydrazination, Density functional theory (DFT).

**Submitted:** September 05, 2019. **Accepted:** October 29, 2019.

**Cite this:** Öztürk I, Şanlıer Ş, Kınal A. Determination of Gluconate Binding Properties on Magnetite Surface and Investigation of Carboxymethylation and Hydrazination Mechanisms of the Gluconated Magnetite Surface: A Computational Study. JOTCSA. 2020;7(1):169–78.

**DOI:** https://doi.org/10.18596/jotcsa.615671.

***Corresponding author.** E-mail:isilayozturk@gmail.com. Telephone: +90 232 311 23 95. Fax: : +90 232 388 82 64.

## INTRODUCTION

Cancer is one of the major dangers to human health. Scientists have been trying to find different strategies employing synergistic effects to kill cancer cells. In recent years, a number of therapeutic and diagnostic agents in nano-biotechnology such as nanocarrier systems for drug delivery (e.g. liposomes, micelles, nanogels, dendrimers, polymeric nanoparticles, and magnetic nanoparticles) have been developed for the treatment of cancer (1-8). One of the biggest challenges for targeted drug delivery practices is to develop nanomolecules that can be loaded with special drugs and can be transported in a simple way (9-11). In this context, magnetite ($Fe_3O_4$) is

the most studied material due to its biocompatibility and sufficient magnetic properties (12-14). When the size of magnetite is on the nanoscale, its magnetic property switches over ferromagnetic to superparamagnetic. This feature enhances the application of magnetite to the biomedical field (6, 15, 16) since they are responsive to an external magnetic field so that they can be directed to specific locations. $Fe_3O_4$ nanoparticles can both agglomerate due to their high magnetic interaction and large surface area, and they can easily be oxidized in a biological environment. These drawbacks can be overcome by coating the magnetite surface with another biocompatible material. The coating of magnetite will also allow drug binding via trapping on the particles, adsorption, or covalent binding (15, 17, 18). Sun et al (19) efficiently synthesized glucose and gluconic acid coated magnetite nanoparticles via a simple and facile hydrothermal reduction route of Fe(III) precursor with sucrose decomposition products. In our laboratories (20), we have also synthesized gluconic acid coated magnetite nanoparticles with the hydrothermal reduction route of Fe(III) proposed by Sun et al (19). In addition, these gluconic acid-coated magnetite nanoparticles were made suitable for carrying doxorubicin drug via carboxymethylation and hydrazination processes. (Experimental details of this study is discussed elsewhere (20).)

In this study, we present computational findings related to the interaction of gluconate molecules with $Fe_3O_4$ nanoparticles as well as carboxymethylation and hydrazination mechanisms of gluconate bound to iron oxide surface. In particular, we investigated the interaction of a gluconate molecule with a model $Fe_6O_8$ surface employing the DFT-B3LYP method and we try to determine binding characteristics of gluconate on the magnetite surface. In addition, we computationally determine the carboxymethylation and hydrazination mechanisms, which makes the nanoparticles ready for drug binding, of the gluconate molecule bound to a modeled magnetite surface.

## COMPUTATIONAL METHODOLOGY

This study consists of two main parts: a) the interaction sites of (binding type) gluconate with modeled magnetite surface; b) the carboxymethylation and hydrazination reaction mechanisms of modeled gluconate molecule bound to magnetite surface. Therefore, different computational methodologies were employed for these parts. In the gluconate-magnetite interaction part, it is needed to create a magnetite surface to model the interaction of gluconate molecules with the magnetite surface. The Cartesian coordinates of the magnetite unit cell with the reverse spinel crystal structure, which will be the basis for this magnetic surface, were obtained from the American Mineralogist Crystal Structure Database, where crystallographic data obtained from X-ray spectroscopy are included (21). Then, we prepared a $Fe_6O_8$ model-magnetite-surface from the Cartesian coordinates of the magnetite unit cell. The reason for the selection of this small size surface is to make its calculation affordable with rather accurate but computationally demanding DFT-B3LYP method that enables us to obtain more plausible binding characteristics. LanL2DZ basis set is employed for both gluconate molecule and the $Fe_6O_8$ surface. Since magnetite nanoparticles are in solid phase, the model $Fe_6O_8$ surface was frozen throughout the optimization.

The B3LYP method was also employed in the second part of the study containing the carboxymethylation and hydrazination reaction mechanisms of the modeled gluconate molecule bound to magnetite surface. Since the gluconate coated iron oxide nanoparticle systems is enormously large for a quantum chemical calculation like DFT methods, the carboxylate anion moiety of gluconate molecule, which binds to positively charged iron atoms of the magnetite surface, were frozen during the DFT calculations. Such modeling does not involve the secondary effects of the iron surface, but it allows the DFT method to be used on the system. All DFT-B3LYP calculations, in all of which the 6-31+G(d,p) basis set was utilized, were performed using the Gaussian 09 program suite. All stationary points on electronic potential energy surfaces of the mechanisms found by optimizations were characterized by the harmonic vibrational frequency calculations. In addition, the transition state (TS) structures were verified by the internal reaction coordinate (IRC) analysis that identifies the correctness of TS structure by following the paths down to both desired reactant and product in the forward and backward directions of the imaginary TS mode. The activation energies of both mechanisms were determined after verification of the TSs by IRC profiles.

## RESULTS AND DISCUSSION

### The Interaction of Gluconate with The Modeled Magnetite Surface

In this section, we aimed to reveal the binding characteristics of gluconate molecules to magnetite surface. There are discussions about binding characteristics of organic acids, especially amino acids, onto magnetite surface in a large number of studies(18, 22-28). The common binding site of organic acid onto magnetite surface referred in all these studies is from the either –COOH or –COO- moiety depending on the pH of the medium. There are three most probable binding structures of –

COO- in basic medium onto magnetite surface: a) monodentate (MB) binding b) bidentate chelating (BC) binding c) bidentate bridging (BB) binding (Scheme 1)(27).

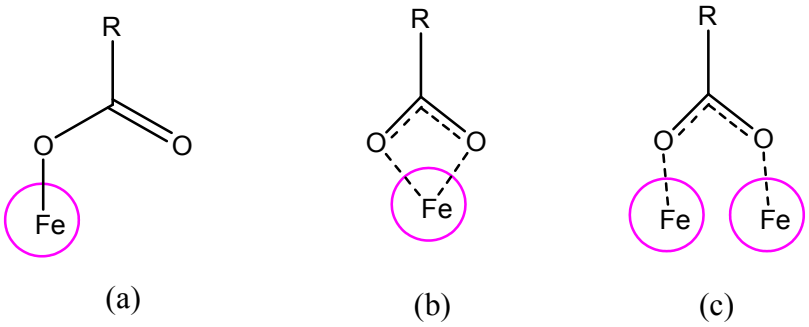


**Scheme 1.** Three most probable binding structure of –COO- onto magnetite surface.

Although there are other methods for binding structure determination such as zeta potential measurements, Raman spectroscopy etc. (26), the most important and widely used binding structure determination method is the vibrational spectroscopy (IR). Free (unbound) carboxylate groups show a symmetric stretch vibration at around 1400 $cm^{-1}$ and an asymmetric stretch vibration at around 1600 $cm^{-1}$(24). There is 200 $cm^{-1}$ difference between symmetric and asymmetric vibrations, Δv, in the unbound state. For –COO- bound to magnetite surface, if Δv is in between 300-400 $cm^{-1}$ then the binding is monodentate (MB), if it is approximately equal to 200 $cm^{-1}$ (150-250 $cm^{-1}$) then the binding is bridged (BB) and finally if it this difference is considerably less than 200 $cm^{-1}$ then it is bidentate chelating (BC) binding (24, 26). Although there are some discrepancies in binding structures of –COO- containing molecules such as carboxylic acids, amino acids, etc., the proposed binding type is either bidentate bridged (BB) or bidentate chelating (BC) type.

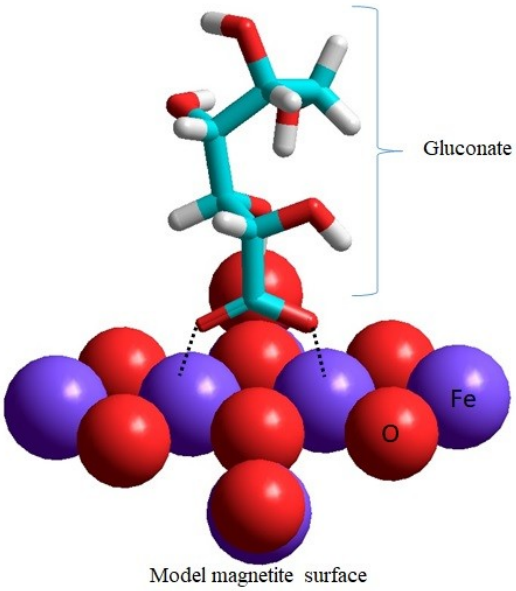


**Figure 1.** The optimized structure of gluconate bonded to model magnetite surface ($Fe_6O_8$) calculated at DFT-B3LYP/LanL2DZ level.

Figure 1 shows the optimized structure of gluconate bonded to model magnetite surface ($Fe_6O_8$) calculated at DFT-B3LYP/LanL2DZ level. The IR spectrum of glucose/gluconate coated magnetite nanoparticles (a) and the computed IR spectrum of the gluconate bonded to model magnetite surface ($Fe_6O_8$) (b) are given in Figure 2. The gluconate coated magnetite nanoparticles synthesized by our group demonstrate IR peaks at 1350 $cm^{-1}$ and 1600 $cm^{-1}$ for symmetric and asymmetric stretch vibrations, respectively, implying that the binding type should be bridged

one (BB) since the difference is slightly higher than 200 $cm^{-1}$. In addition to that, the DFT-B3LYP calculations on bridged bonded gluconate on modeled magnetite surface revealed IR peaks at 1350 $cm^{-1}$ and 1521 $cm^{-1}$ for symmetric and asymmetric stretch vibrations, respectively, confirming the experimental findings. Consequently, the gluconate is most probably bonded to the magnetite surface through bidentate bridged binding as indicated both experimental and theoretical findings.

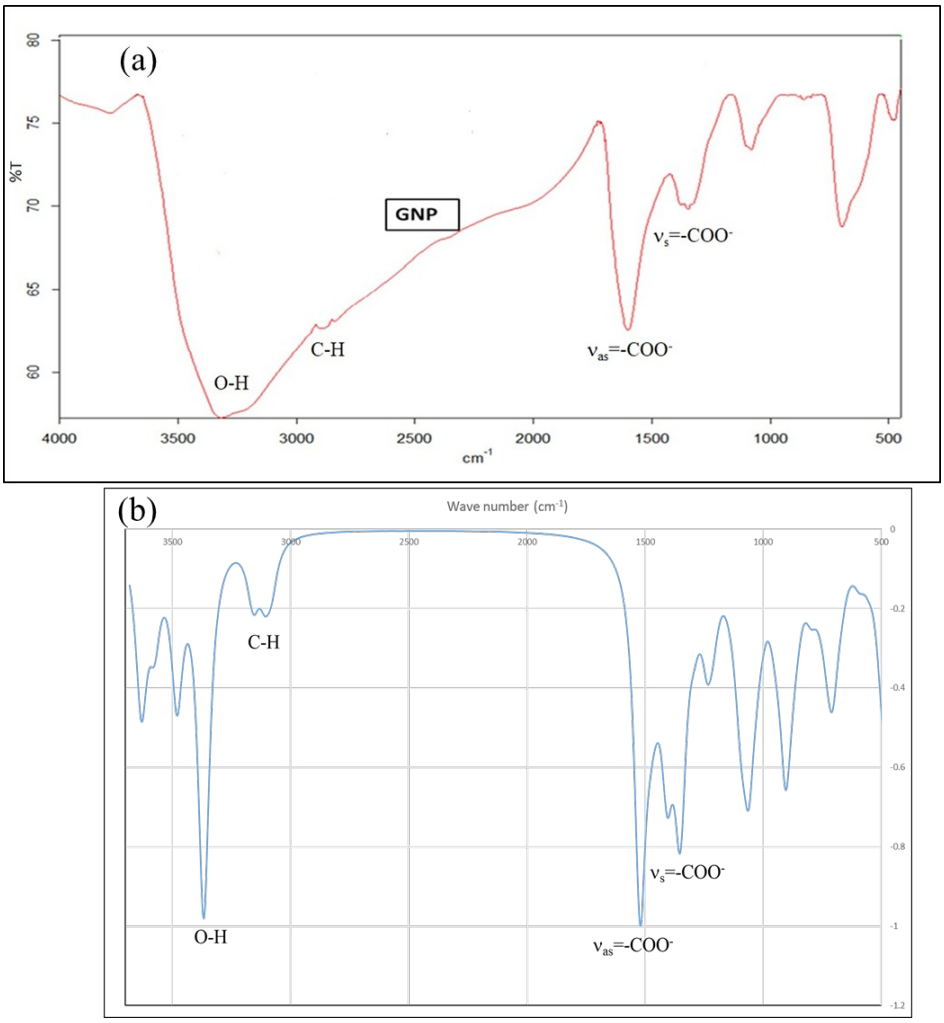


**Figure 2.** (a) the IR spectrum of glucose/gluconate coated magnetite nanoparticles and (b) the computed IR spectrum of the gluconate bonded to model magnetite surface ($Fe_6O_8$).

**The Carboxymethylation Mechanism of The Gluconate Bound To Modeled Magnetite Surface**

The experimental carboxymethylation procedure of gluconate coated magnetite nanoparticles occurs in a highly basic medium at elevated temperature (about 70 ºC) (20). Therefore, the base form of chloroacetic acid were used in the calculations. The mechanism proposed for the carboxymethylation reaction of gluconate coated iron oxide nanoparticle model and its energetics aqueous medium calculated at B3LYP/6-31+G(d,p) level are given in Figures 3 and 4, respectively.

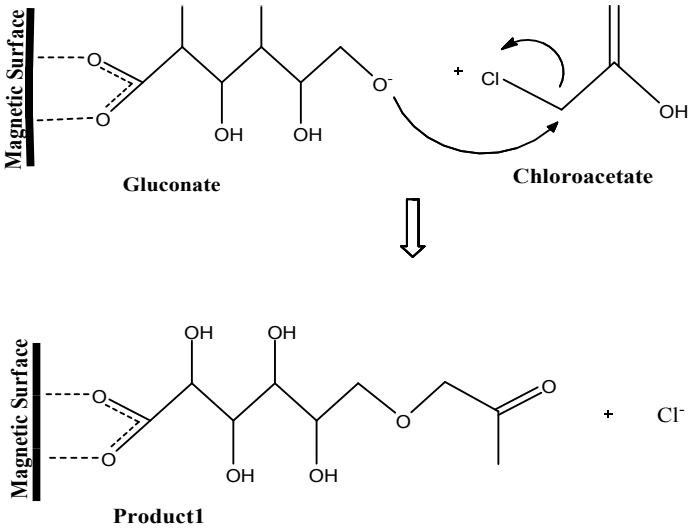


**Figure 3.** Mechanism of carbonyl group attached on gluconate bonded to magnetite surface.

The reaction between gluconate and chloroacetate occurring in the aqueous medium is well-known single-step nucleophilic substitution reaction ($SN_2$). As seen from Figure 4, the nucleophilic O1 atom, which has a Mulliken charge of -0.927e, the gluconate of molecule attacks the primer C1 atom (-0.377e, aliphatic $sp^3$ carbon center) of the chloroacetic acid. In the TS structure formed, while these atoms come close to each other (the distance between O1 and C1 is 2.319 Å), chlorine atom leaves the molecule as a chloride ion (the distance between C1 and Cl1 is 2.156 Å). Hence, the carboxymethylated gluconate (product1) is obtained. Experimentally, this reaction takes place relatively quickly (2-6 hours) under moderate conditions (at 70 ºC and atmospheric pressure). The DFT method predicts the activation energy of the reaction to be 12.3 kcal/mol and the reaction enthalpy to be –42.8 kcal/mol. The low activation barrier and the exothermic nature of the reaction can be attributed to the fact that the carboxymethylation reaction is relatively easy under moderate conditions.

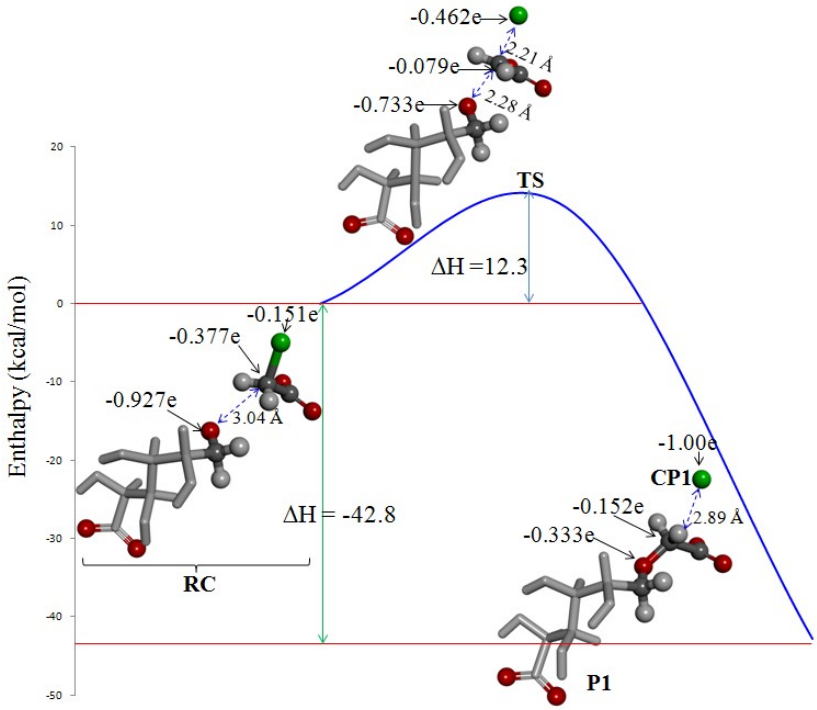


**Figure 4.** Energy profile (in kcal/mol) of carboxymethylation mechanism in water. Some important Mulliken partial charges on atoms are also given (RC: reactants; P1: product2; CP1: Cleaved part from TS).

**The Hydrazination Mechanism of The Modeled Carboxymethylated Gluconate Bound To Magnetite Surface**

The hydrazination reaction starts when P1 (the carboxymethylated gluconate) is reacted with EDC [1-ethyl-3-(3-dimethylaminopropyl) carbodiimide] and hydrazine, consecutively. According to the literature (29), this reaction occurs in two steps. Figure 5 shows the reagents, intermediates, and products involving in this reaction. In the first step of the mechanism, P1 was interacted with EDC to form the intermediate (o-acyl isourea). In the second step where a Wolff-Kishner's reduction actually takes place (30), this intermediate reacts with hydrazine molecule to form the product2.

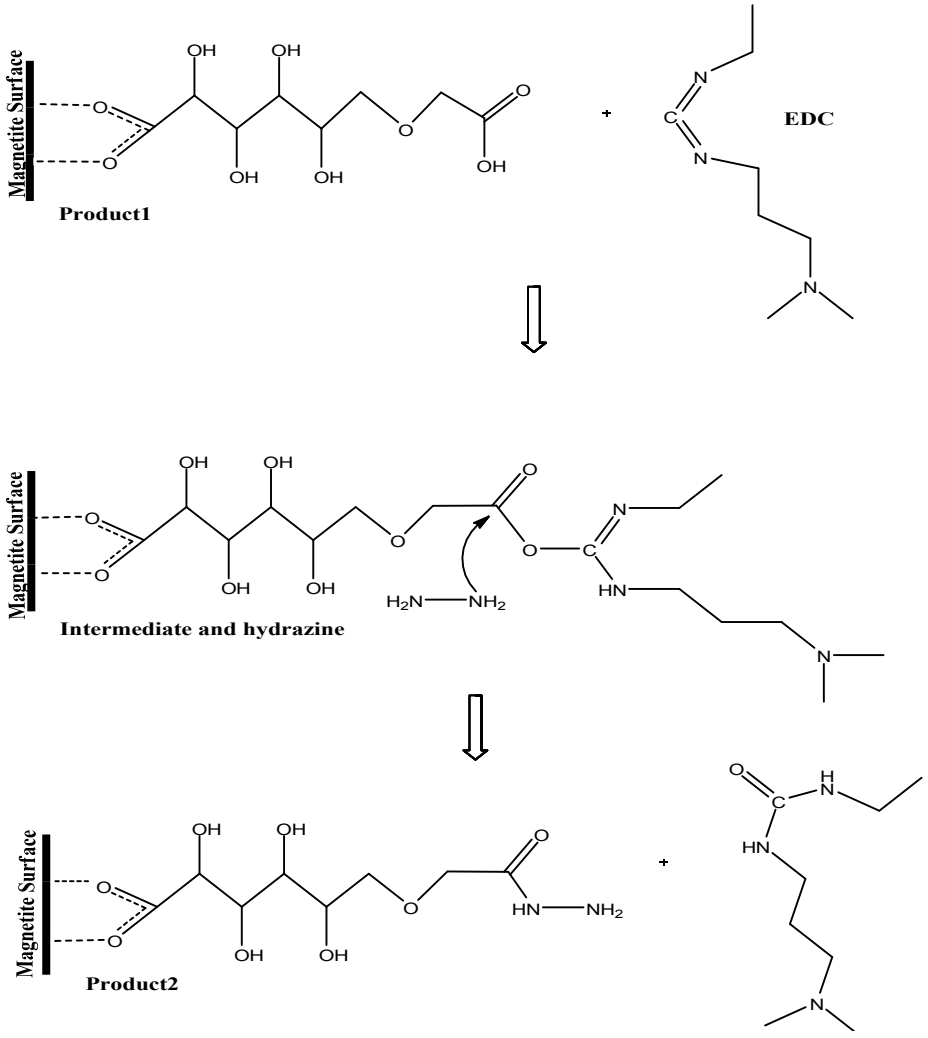


**Figure 5.** Hydrazine mechanisms in two-stage of product1.

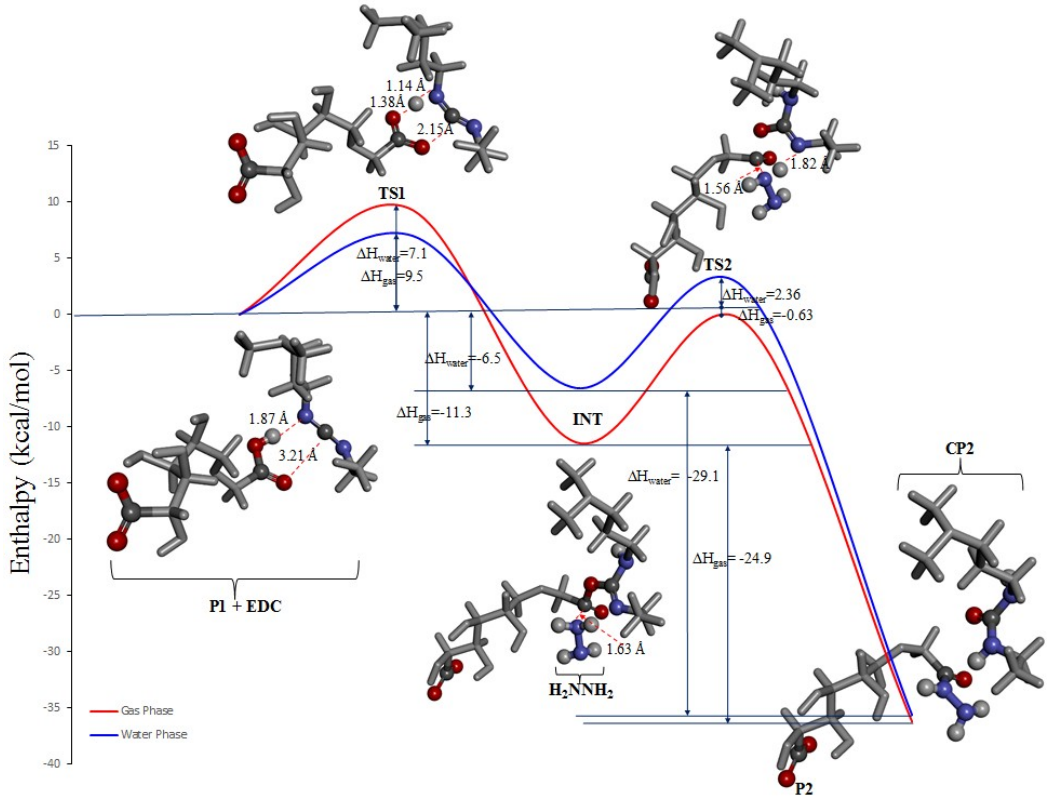


**Figure 6.** Hydrazination mechanism occurring in two steps (RC: reactants; INT: intermediate; P2: product2; CP2: Cleaved part from TS2).

The reactant, TS, intermediate and product geometries involved in the hydrazination reaction mechanism, activation barriers and reaction enthalpies calculated at B3LYP/6-31+G(d,p) level are given in Figure 6. Activation barriers of first and second steps of the hydrazination reaction with respect to the reactant molecules are found to be 7.1 kcal/mol and 2.4 kcal/mol in water (9.5 kcal and -0.63 kcal in the gas phase), respectively. In a multistep mechanism, the step with the highest energy TS is called the rate-determining step. Accordingly, the activation energy of the first step is greater than that of the second step, so the overall reaction activation barrier predicted by the DFT method is the barrier of the first step (7.1 kcal/mol). In addition, the DFT method predicted that both the first step and the second step of the reaction is highly exothermic. Low barrier and high exothermicity indicate that this reaction can occur rather easily without the need for heat. Experimentally, this reaction takes place relatively quickly (4 hours) under ordinary conditions (at 25 °C and atmospheric pressure). Consequently, the results of the calculations completely agree with the experimental findings.

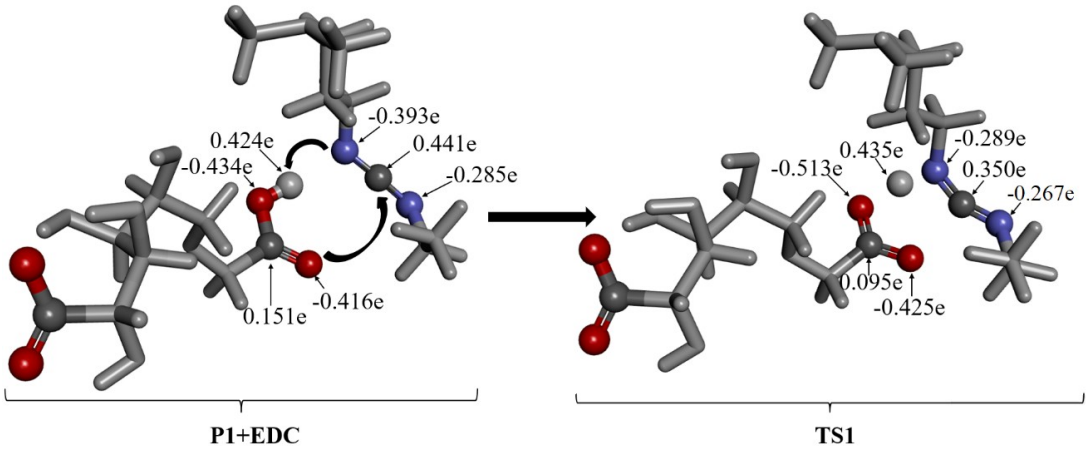

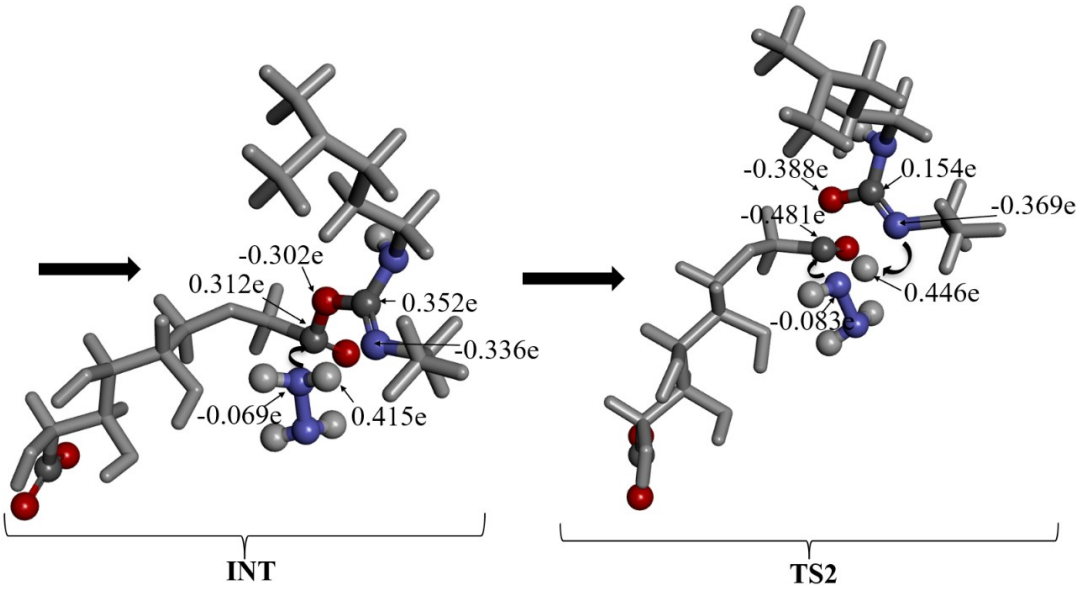


**Figure 7.** Optimized geometries and important Mulliken partial charges of the species involved in the first and second steps of hydrazination mechanism.

In the first step, the H atom (0.424e) of carboxylic acid moiety of P1 transfers onto the N (-0.393e) atom of carbondiimide part of the EDC molecule while the C atom (0.441e) of carbondiimide part of the EDC molecule interacts with the O atom (-0.416e) of carboxylic acid moiety of P1 to form the o-acyl iso urea intermediate (Figure 7). This step is an exothermic one with a reaction enthalpy of -6.5 kcal/mol in water (-11.3 kcal/mol in the gas phase).

In the second step, the N atom (-0.069e) of hydrazine molecule attacks the C atom of the carbonyl group of the o-acyl iso urea intermediate (INT), then an instant zwitterionic intermediate formation occurs and this attack ends with the removal of the iso-urea derivative. Meanwhile, one proton (0.446e) coming from hydrazine is transferred to the N atom (-0.369e) of the iso-urea derivative. This reaction is known as the Wolff-Kishner reduction (30). The second step is also an exothermic step with a reaction enthalpy of -29.1 kcal/mol in water and -24.9 kcal/mol in the gas phase. As a result of these two exothermic steps, the P1 is converted into P2 via carboxylic acid to an amide (hydrazine addition). Since the DFT calculations predict the overall reaction enthalpy of hydrazination reaction as -35.6 kcal/mol in water and -36.2 kcal/mol in the gas phase, it can be concluded that this reaction occurs spontaneously at room temperature.

## CONCLUSION

In this article, we first determined the binding properties of a gluconate molecule to the model magnetite surface. We then investigated the carboxymethylation and hydrazination mechanisms of gluconate bound to the magnetite surface employing the DFT-B3LYP method. When the computationally determined IR spectra of the gluconate molecule interacting with the model Fe6O8 surface are investigated, the bonding type is found to be the bidentate bridging binding. This is also confirmed with the experimental IR spectra obtained from the gluconated iron oxide nanoparticles. For the carboxymethylation reaction, the calculation results are revealed that the reaction between gluconate and chloroacetate has one step mechanism passing through a low activation barrier and that the reaction is exothermic. Therefore, the carboxymethylation reaction can be said to be relatively easy to perform under moderate conditions. On the other hand, the hydrazination reaction is found to be a two-step reaction. The DFT calculations show the activation energy barrier of the former step being higher than that of the latter step, leading to the fact that the rate determining step is the first step. They also reveal that the hydrazination reaction can be carried out spontaneously at room temperature due to both steps being considerably exothermic. This finding is also confirmed by the experimental data.

## ACKNOWLEDGMENT

The authors thank the Scientific and Technological Research Council of Turkey (TUBITAK) (Project ID: 113Z165) and Ege University Scientific Research Project Office (Project ID: 2014 BIL 006 and 2015 FEN 055) for their financial support. All calculations reported in this paper were performed at High Performance and Grid Computing Center (TRUBA resources), ULAKBIM. IO acknowledges the contrubitions of Guliz Ak and Habibe Yılmaz.

**REFERENCES**

1. Manchun S, Dass CR, Sriamornsak P. Targeted therapy for cancer using pH-responsive nanocarrier systems. Life Sci. 2012;90(11–12):381–7.

2. Wei H, Zhuo RX, Zhang XZ. Design and development of polymeric micelles with cleavable links for intracellular drug delivery. Prog Polym Sci. 2013;38(3–4):503–35.

3. Etrych T, Kovář L, Strohalm J, Chytil P, Říhová B, Ulbrich K. Biodegradable star HPMA polymer-drug conjugates: Biodegradability, distribution and anti-tumor efficacy. J Control Release. 2011;154(3):241–8.

4. Chang Y, Meng X, Zhao Y, Li K, Zhao B, Zhu M, vd. Novel water-soluble and pH-responsive anticancer drug nanocarriers: Doxorubicin-PAMAM dendrimer conjugates attached to superparamagnetic iron oxide nanoparticles (IONPs). J Colloid Interface Sci. 2011;363(1):403–9.

5. Deng C, Jiang Y, Cheng R, Meng F, Zhong Z. Biodegradable polymeric micelles for targeted and controlled anticancer drug delivery: Promises, progress and prospects. Nano Today. 2012;7:467–80.

6. Jun YW, Huh YM, Choi JS, Lee JH, Song HT, Kim S, vd. Nanoscale Size Effect of Magnetic Nanocrystals and Their Utilization for Cancer Diagnosis via Magnetic Resonance Imaging. J Am Chem Soc. 2005;127(16):5732–3.

7. Uribe Madrid SI, Pal U, Kang YS, Kim J, Kwon H, Kim J. Fabrication of Fe3O4 @mSiO2 Core-Shell Composite Nanoparticles for Drug Delivery Applications. 2011;

8. Ray Chowdhuri A, Bhattacharya D, Sahu SK. Magnetic nanoscale metal organic frameworks for potential targeted anticancer drug delivery, imaging and as an MRI contrast agent. Dalt Trans. Royal Society of Chemistry; 2016;45(7):2963–73.

9. Singh R, Lillard JW. Nanoparticle-based targeted drug delivery. Exp Mol Pathol. 2009;86(3):215–23.

10. Paper R, Manish G, Vimukta S. Targeted drug delivery system : A Review. Res J Chem Sci ResJChemSci. 2011;1(2):1–24.

11. Zhang L, Li Y, Yu JC. Chemical modification of inorganic nanostructures for targeted and controlled drug delivery in cancer treatment. J Mater Chem B. 2014;2(5):452–70.

12. Arruebo M, Fernández-Pacheco R, Ibarra MR, Santamaría J. Magnetic nanoparticles for drug delivery. June. 2007;2(3).

13. Sun C, Lee JSH, Zhang M. Magnetic nanoparticles in MR imaging and drug delivery. Adv Drug Deliv Rev. 2008;60(11):1252–65.

14. McCarthy JR, Weissleder R. Multifunctional magnetic nanoparticles for targeted imaging and therapy. Adv Drug Deliv Rev. 2008;60(11):1241–51.

15. Uribe Madrid SI, Pal U, Kang YS, Kim J, Kwon H, Kim J. Fabrication of Fe3O4@mSiO2 Core-Shell Composite Nanoparticles for Drug Delivery Applications. Nanoscale Res Lett. Aralık 2015;10(1):217.

16. Akbarzadeh A, Samiei M, Davaran S. Magnetic nanoparticles: Preparation, physical properties, and applications in biomedicine. Nanoscale Res Lett. 2012;7(1):144.

17. Harris LA, Goff JD, Carmichael AY, Riffle JS, Harburn JJ, St. Pierre TG, vd. Magnetite nanoparticle dispersions stabilized with triblock copolymers. Chem Mater. 2003;15(6):1367–77.

18. Chen C, Jiang X, Kaneti YV, Yu A. Design and construction of polymerized-glucose coated Fe3O4magnetic nanoparticles for delivery of aspirin. Powder Technol. Elsevier B.V.; 2013;236:157–63.

19. Sun X, Zheng C, Zhang F, Yang Y, Wu G, Yu A, vd. Size-controlled synthesis of magnetite (Fe3O4) nanoparticles coated with glucose and gluconic acid from a single Fe(III) precursor by a sucrose bifunctional hydrothermal method. J Phys Chem C. 2009;113(36):16002–8.

20. Ak G, Yilmaz H, Güneş A, Hamarat Sanlier S. In vitro and in vivo evaluation of folate receptor-targeted a novel magnetic drug delivery system for ovarian cancer therapy. Artif Cells, Nanomedicine, Biotechnol. Informa UK Limited, trading as Taylor & Francis Group; Şubat 2018;0(0):1–12.

21. Haavik C, Stølen S, Fjellvåg H, Hanfland M, Häusermann D. Equation of state of magnetite and its high-pressure modification: Thermodynamics of the Fe-O system at high pressure. Am Mineral. 2000;85(3–4):514–23.

22. Salafranca J, Gazquez J, Pérez N, Labarta A, Pantelides ST, Pennycook SJ, vd. Surfactant organic molecules restore magnetism in metal-

oxide nanoparticle surfaces. Nano Lett. 2012;12(5):2499–503.

23. Demir A, Topkaya R, Baykal A. Green synthesis of superparamagnetic Fe3O4 nanoparticles with maltose: Its magnetic investigation. Polyhedron. Elsevier Ltd; 2013;65:282–7.

24. Schwaminger SP, García PF, Merck GK, Bodensteiner FA, Heissler S, Günther S, vd. Nature of Interactions of Amino Acids with Bare Magnetite Nanoparticles. J Phys Chem C. 2015;119(40):23032–41.

25. Nosrati H, Salehiabar M, Davaran S, Ramazani A, Manjili HK, Danafar H. New advances strategies for surface functionalization of iron oxide magnetic nano particles (IONPs). Res Chem Intermed. Springer Netherlands; 2017;43(12):7423–42.

26. Schwaminger SP, Blank-Shim SA, Scheifele I, Fraga-García P, Berensmeier S. Peptide binding to metal oxide nanoparticles. Faraday Discuss. 2017;

27. Śmiłowicz M, Pogorzelec-Glaser K, Łapiński A, Motała R, Grobela M, Andrzejewski B. Spectroscopic and quantum chemical studies of interaction between the alginic acid and Fe<inf>3</inf>O<inf>4</inf> nanoparticles. Spectrochim Acta - Part A Mol Biomol Spectrosc. 2017;182:1–7.

28. Sanchez LM, Martin DA, Alvarez VA, Gonzalez JS. Polyacrylic acid-coated iron oxide magnetic nanoparticles: The polymer molecular weight influence. Colloids Surfaces A Physicochem Eng Asp. Elsevier; 2018;543(December 2017):28–37.

29. Custer TG, Kato S, Bierbaum VM, Howard CJ, Morrison GC. Gas-Phase Kinetics and Mechanism of the Reactions of Protonated Hydrazine with Carbonyl Compounds . Gas-Phase Hydrazone Formation : Kinetics and Mechanism. 2004;1(2):2744–54.

30. Taber DF, Stachel SJ. On the mechanism of the Wolff-Kishner reduction. Tetrahedron Lett. Pergamon; Şubat 1992;33(7):903–6.